A Photonic Bandgap (PBG) Structure for Guiding and Suppressing Surface Waves in Millimeter-Wave Antennas

Young-Jin Park, *Student Member, IEEE,* Alexander Herschlein, and Werner Wiesbeck, *Fellow, IEEE*

***Abstract*—Periodic and regular metal posts, a photonic bandgap (PBG) structure for guiding surface waves in a parallel-plate waveguide is proposed. The isotropic PBG structure is applied to the design of an asymmetric parallel-plate waveguide Luneburg lens (APWLL). The relation between the dimensions of the metal posts and the required refraction index in the lens is derived with the transmission-line theory and the transverse resonance method. Different lattices for the entire lens are also investigated. For verification, an antenna for a 76.5 GHz adaptive-cruise-control radar is fabricated, consisting of an APWLL, a primary feed, and symmetric corrugated flares to improve the property of the antenna in elevation. Measured results verify the PBG structure design in the APWLL.**

***Index Terms*—Adaptive cruise control radar, electromagnetic bandgap, Luneburg lens antennas, millimeter-wave antennas, photonic bandgap.**

I. Introduction

In ANTENNA designs, photonic bandgap (PBG) structures [1] are often used for suppressing surface waves and high-impedance ground plane for electrically thin antennas. As is well known, for the above applications, PBG structures make use of their property of high-impedance near resonance frequency f_0 [2], [3]. Sometimes, the frequency band near f_0 is called electromagnetic bandgap (EBG) for microwave or millimeter (mm)-wave frequencies [4].

In addition to the high-impedance near f_0, PBG structures have the interesting property of supporting arbitrary surface impedances in lower and higher frequencies than f_0 [2], [3]. For antenna applications, this property can be well applied to guide surface waves and to replace dielectrics in lens antennas [5]. Certainly, these facts of PBG structures are not new or surprising since periodic structures like corrugated surfaces and artificial dielectrics have already been used for those applications [5]–[9]. In recent years, while investigating and applying many PBG structures, little interest in the property of PBG structures has been shown despite their good applications for antennas. However, there is no doubt that cultivating the attractive property of PBG structures in lower or higher frequencies is a very interesting subject.

This paper presents a PBG structure for guiding surface waves by regular and periodic metal posts in a parallel-plate waveguide and shows an application to the design of an asymmetric parallel-plate waveguide Luneburg lens (APWLL).

The relation between surface impedances and post dimensions is calculated with the transmission-line theory and the transverse resonance method (TRM). For the design of an APWLL, the radiation pattern of the APWLL is predicted with geometrical optics (GO) and the aperture integral method. For the proper lattices for the APWLL, several lattices are investigated with the aid of HFSS.[1] Finally, with the APWLL, an antenna for a 76.5-GHz adaptive cruise control (ACC) radar is manufactured to verify the simulation and design procedure. The complete antenna system is composed of an APWLL, a pair of rotationally symmetric corrugated flares, and a primary feed. The APWLL forms the beams in azimuth. To satisfy the requirements for the ACC radar in elevation [10], a pair of rotationally symmetric corrugated flares are added. As a primary feed, a H-plane sectoral horn is chosen. Measured results verify the PBG structure's property to substitute the function of a Luneburg lens and the design procedure of the antenna.

In Section II, characteristics of dielectrics in a Luneburg lens are outlined. In Section III, the PBG structure is discussed. In Sections IV and V, the design and fabrication procedures of an APWLL, a pair of rotationally symmetric corrugated flares and a primary feed are presented. Several measured results and conclusions close the paper.

II. Parallel-Plate Waveguide Luneburg Lens

In Fig. 1(a), a cross-sectional view of a parallel-plate waveguide Luneburg lens, called a TEM flat-plate Luneburg lens is illustrated. As is well known, the lens requires the refraction index profile ($n(r')$), i.e.,

$$n(r') = \sqrt{2 - r'^2}, \qquad 0 \le r' \le 1$$
$$n(r') = 1, \qquad r' \ge 1 \tag{1}$$

where r' is the normalized radius [11]. With the refraction index in (1), a cylindrical wave from a primary feed is transformed into a plane wave as shown in Fig. 1(b). In the TEM flat-plate Luneburg lens, the thickness of isotropic homogeneous dielectric is varied in a radial direction to satisfy the index profile.

This lens is considered as a promising device for use in wide angle scanning applications which require a thin lens [12]. However, the lens in Fig. 1(a) is somewhat difficult to realize due to

Manuscript received January 5, 2001; revised May 25, 2001.

The authors are with the Institut für Höchstfrequenztechnik und Elektronik, Universität Karlsruhe, D-76128 Karlsruhe, Germany (e-mail: yjpark@ieee.org).

Publisher Item Identifier S 0018-9480(01)08728-2.

[1]HFSS version 2.0.55, Ansoft Corporation, Pittsburgh, PA, 1999.

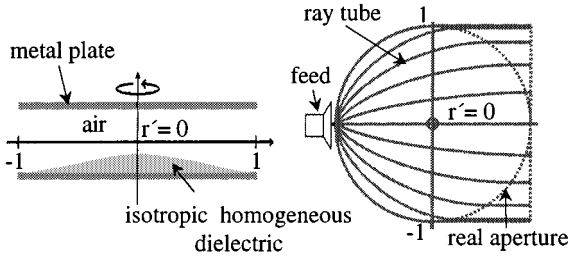

(a) (b)

Fig. 1. TEM flat-plate Luneburg lens. (a) Cross-sectional view. (b) Top view and ray tube in the lens.

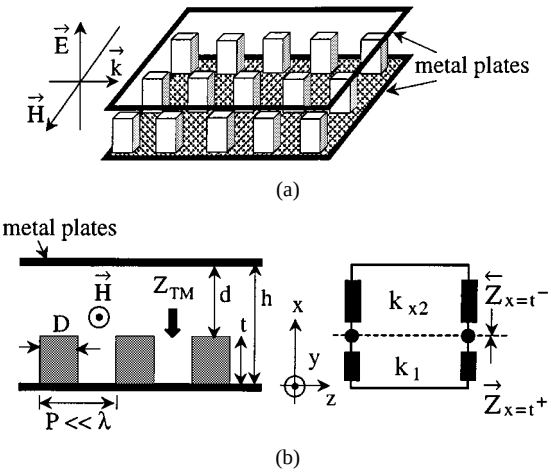

Fig. 2. Geometry of the PBG structure. (a) Periodic and regular metal posts in a parallel-plate waveguide. (b) Cross-sectional view and transverse resonance equivalent circuit of the structure.

the stability and interface between dielectric and metal in millimeter frequencies. To overcome the problems, a metallic PBG structure which supports arbitrary surface impedances like the dielectric in the lens is introduced.

III. Periodic, Regular Metal Posts

Fig. 2(a) shows regular and periodic metal posts in a parallel-plate waveguide. In [5], [13], and [14], it has been demonstrated that periodic metal posts have arbitrary surface impedances and guide surface waves.

In Fig. 2(b), the cross-sectional view of the PBG structure and its transverse resonance equivalent circuit are presented. At first, for the surface impedance, it is assumed that only a TEM mode exists between the posts under the conditions $\mathrm{P(period)} \ll \lambda$ (a wavelength in the medium between the posts) and post-width $\mathrm{D} \leq \mathrm{P}/2$. Using the transmission-line theory and considering post dimensions, the surface impedance is derived as

$$Z_{\mathrm{TM}} = jW\eta_1 \tan(k_1 t) \tag{2}$$

where $\eta_1 = \sqrt{\mu_0/(\varepsilon_0\varepsilon_{r1})}$, $k_1 = 2\pi/\lambda$, and $W = (\mathrm{P} - \mathrm{D})/\mathrm{P}$ is the ratio of the length unfilled by the post to the period. Note that the equation of the surface impedance is consistent with that of the corrugated surface in [15]. However, since the PBG structure has an isotropic property, it is distinguished from the corrugated surfaces. With post heights near $t = (2m + 1)\lambda/4(m = 0, 1, 2, \ldots)$, the structure has a high impedance regardless of W and then is used to suppress surface waves. In case $(2m+1)\lambda/4 < t < (2m+2)\lambda/4$, called forbidden band for transverse magnetic (TM) surface waves, the structure has a capacitive surface impedance regardless of W, therefore it will suppress TM surface waves. On the contrary, at lower frequencies where $2m\lambda/4 < t < (2m+1)\lambda/4$, the surface impedance becomes inductive, so that the structure is used to guide TM surface waves. Conclusively, the PBG structure can generate arbitrary surface impedances and suppress or guide surface waves.

The relation between surface impedance and post dimensions is obtained using the TRM. From the transverse resonance condition, the sum of two impedances $\overrightarrow{Z}_{x=t^+}$ and $\overleftarrow{Z}_{x=t^-}$ in Fig. 2 should be zero on the resonance line, i.e., $\overrightarrow{Z}_{x=t^+} + \overleftarrow{Z}_{x=t^-} = 0$. $\overleftarrow{Z}_{x=t^-}$ has been already given as Z_{TM}. Also, the transmission-line theory leads to $\overrightarrow{Z}_{x=t^+}$ as

$$\overrightarrow{Z}_{x=t^+} = j\frac{k_{x2}}{\omega\varepsilon_0\varepsilon_{r2}} \tan(k_{x2}(h-t)) \tag{3}$$

with $k_{x2} = \sqrt{k_2^2 - k_{z2}^2}$ and $k_2 = \omega\sqrt{\mu_0\varepsilon_0\varepsilon_{r2}}$. Now consider the PBG structure as a dielectric whose dielectric constant is ε_r, so that k_{x2} is written as $k_0\sqrt{\varepsilon_{r2} - \varepsilon_r} = k_0\sqrt{\varepsilon_{r2} - n^2}$ where n is a refraction index and $k_0 = \omega\sqrt{\mu_0\varepsilon_0}$. With $\varepsilon_{r2} > n^2$, the PBG structure cannot support surface waves any more. Therefore, for the goal of guiding surface waves, $k_{x2} = adjk_0\sqrt{n^2 - \varepsilon_{r2}}$ is put into (3) and then $\overrightarrow{Z}_{x=t^+} + \overleftarrow{Z}_{x=t^-} = 0$ is written as

$$\sqrt{n^2 - \varepsilon_{r2}} \tanh\Big(k_0\sqrt{n^2 - \varepsilon_{r2}}(h-t)\Big) = \frac{\varepsilon_{r2}}{\sqrt{\varepsilon_{r1}}} W \tan(k_1 t). \tag{4}$$

This equation is numerically solved for the desired post heights t. As a simple example, if air is filled in the entire structure and h goes to infinity, that is, without the upper plate, k_{z2} becomes $k_0\sqrt{1 + (W\tan(k_0 t))^2}$ as given in [14] and [15].

IV. Simulation and Design

A. APWLL

The above PBG design is applied to an APWLL for a 76.5-GHz ACC radar. To calculate the post heights which satisfy the required refraction index in (1), the index is simply put in (4) and air is filled in the parallel-plate waveguide, i.e., $\varepsilon_{r1} = \varepsilon_{r2} = 1$ in (4).

In Fig. 3, three normalized post profiles t are plotted as functions of spacings of the waveguide h. With larger h, the profile becomes higher. But with h larger than $\lambda/2$, the post height t is little changed. It means that with larger h, small deviation of h in fabrication and measurement will have little influence on the lens performance. However, if $h > \lambda/2$, higher modes near the rim of the lens may be excited. Therefore, by considering the above effects, h should be determined in a APWLL design. Additionally, it is necessary to note that at millimeter frequencies, h and the entire profile of the posts are very low.

To obtain the goal of a wide beam scanning, an isotropic property of the PBG structure is strongly required. The performance of an isotropic property of the PBG structure is closely related to lattices. Several lattices such as a hexagonal lattice, a square lattice, and a triangular lattice are investigated with the aid of

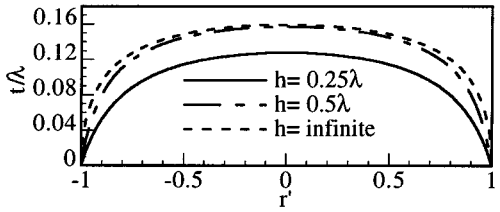

Fig. 3. Normalized post profiles as functions of spacings of the waveguide h. $\mathrm{P} = 0.2\lambda$ and $\mathrm{D} = 0.07\lambda$.

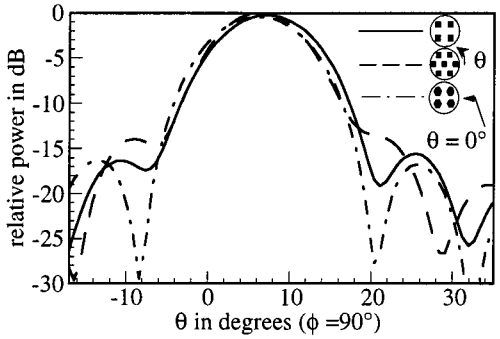

Fig. 4. H-plane radiation patterns calculated by HFSS in case of three different lattices.

HFSS. In simulation, the operating frequency is 76.5 GHz and a H-plane sectoral horn 3.6 mm $\times$ 1.9 mm is used. With consideration of computation time, the APWLL's diameter of 5.1λ is chosen. Also by considering the mechanical stability in fabrication and the conditions for only the TEM mode given in Section III, the proper parameters are determined to $\mathrm{P} = 0.78$ mm and $rmD = 0.28$ mm. The parallel-plate spacing $h = 1.9$ mm is chosen to reduce the sensitivity by the deviation of the spacing h and suppress higher modes near the rim of the APWLL.

Fig. 4 illustrates the H-plane radiation patterns (at $\phi = 90°$) of three cases: square lattice with square posts, hexagonal lattice with square posts, and square lattice with hexagonal posts. To grant the arbitrariness of a scan angle, they are simulated at a random scan angle of $\theta = 6°$. The simulation shows that the square lattice with square posts or hexagonal posts are better than the hexagonal lattice with square posts. However, the determination is to fabricate an APWLL with the square lattice with square posts due to its simpler fabrication in lab. In terms of E-plane radiation patterns (at $\phi = 0°$) of the three cases, the patterns are nearly the same, so that for comparison with the measurement, only the pattern in case of the square lattice is illustrated in Fig. 9.

B. Primary Feed

To decide the feed dimension, the relations between feed dimensions and both the desired half power beam width (HPBW) and the sidelobe levels are investigated by calculating the radiation patterns of the APWLL in azimuth. To get the pattern, first, the field on the real aperture of the APWLL is calculated with GO. Second, the aperture integration method leads to a radiation pattern applying the real aperture field calculated by GO previously [16]. In this paper, for a HPBW of about 5° and the first sidelobe < -18 dB in case of the APWLL with a 50-mm diameter, a H-plane sectoral horn with an aperture of 3.6 mm $\times$ 1.27 mm is determined by the proper dimension. The simulation result with the feed horn and the 50 mm APWLL is shown in Fig. 8.

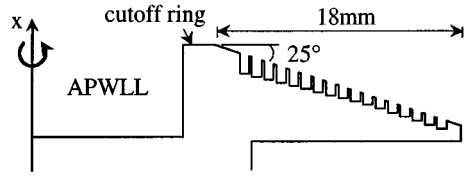

Fig. 5. Cross-sectional view of the rotationally symmetric corrugated flare.

C. Rotationally Symmetric Corrugated Flares

A pair of rotationally symmetric corrugated flares are added to the APWLL to achieve a desired HPBW and low sidelobe levels in elevation. As illustrated in Figs. 5 and 7, the flares and the APWLL can be separated. Since they are rotationally symmetric, the entire antenna retains the property of the APWLL, like a wide scan angle and multiple beam. Also, to suppress higher modes near the rim of the APWLL, a cutoff ring is placed between the end of the APWLL and the throat of the flares.

In the simulation of the flares, it is assumed that the field distribution at the flares is the same cosine distribution as that of corrugated pyramidal horns in E-plane. Now, the E-plane radiation patterns are calculated by the aperture integration method without considering the edge diffraction [17]. For the HPBW of 20°, 22.1 mm and 25° are chosen as the optimum flare length and flare angle, respectively. The simulation result is shown in Fig. 11.

For the design of the corrugation, the design procedure of corrugated horns in [18] is followed. First, to suppress TM surface waves, the depth of the teeth should be between $\lambda/4$ and $\lambda/2$. Second, by considering the mechanical stability and electronic properties such as low power loss and low reflection, the width of the teeth 0.2 mm and the period 0.9 mm are selected. As shown in Fig. 5, the depth near the throat of the flare is about $\lambda/2$ and that near the end of the flare about $\lambda/4$ in order to reduce the reflection at the transition of the flare throat. In other words, corrugations with depth of $\lambda/2$ near the flare throat act like a conducting surface while corrugations with $\lambda/4$ depth present a high impedance.

Note that wave propagation is not perpendicular to the circular corrugations in case that $\phi \neq 0°$ with a scan angle 0° (see Figs. 5 and 7). However, the corrugations will suppress surface waves well because the capacitive surface impedance is dependent on only the depth of the teeth regardless of W.

V. Fabrication

A. Fabrication of an APWLL

The APWLL is composed of two aluminum plates. One plate is a plain aluminum plate, and the other is provided with the PBG structure on the surface. As determined in Section IV, the width of square posts $\mathrm{D} = 0.28$ mm and the period $\mathrm{P} = 0.78$ mm. The spacing h of the parallel-plate waveguide is 1.9 mm. The lattice is square. The APWLL's diameter is 50 mm.

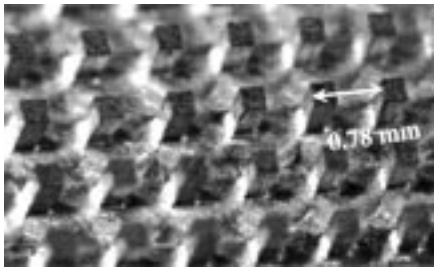

Fig. 6. Photograph of the PBG structure in the APWLL.

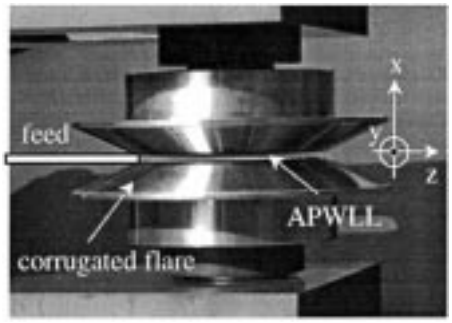

Fig. 7. Experimental setup.

The fabrication of the plate with the PBG structure is divided into three steps. First, the metal surface curvature is fabricated on a computer numeric control (CNC) revolving machine with the data of the post height obtained using (4). The machine has the tolerance of 1 μm. Second, a CNC milling machine produces the posts by machining the curve. In the end, it is etched by an acid to get away the metal wastes between the posts and around the posts. It consists of about 3000 square posts. In Fig. 6, a picture of some part of the APWLL taken is presented to show the appearance of posts. As illustrated in Fig. 6, square posts are arranged periodically and regularly. Also, the APWLL has a square lattice. In contrast, the plain aluminum plate for the other plate is produced by the CNC revolving machine with diamond cutter. The plate looks like a plain metal mirror.

B. Fabrication of a Primary Feed

Using an end-fire WR-10 waveguide, the H-plane sectoral horn with an aperture of 3.6 mm $\times$ 1.27 mm is implemented (the outside dimension is 4.6 mm $\times$ 1.9 mm). Both, upper and lower outer copper walls are machined carefully to make the entire height of the horn become the same as the plate spacing $h = 1.9$ mm, due to the region of the cutoff ring (see Fig. 5). Thus, in measurement, the aperture of the horn is placed in the middle of the parallel-plate waveguide.

C. Fabrication of Symmetric Corrugated Flares

In Figs. 5 and 7, the rotationally symmetric corrugated flare is presented. The fabrication of the flares is divided into two steps. First, the CNC revolving machine fabricates the plain flares which look like a biconical antenna, and then the circular corrugations are engraved on the flares. A cutoff ring 2.2 mm is placed at the rim of the APWLL. Each flare has 17 corrugations.

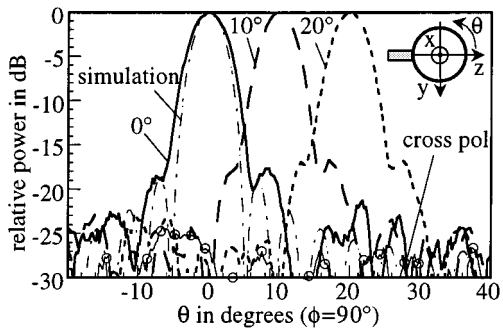

Fig. 8. H-plane radiation patterns for three different scan angles without the corrugated flares and simulation result. Cross polarization at a scan angle of 0°.

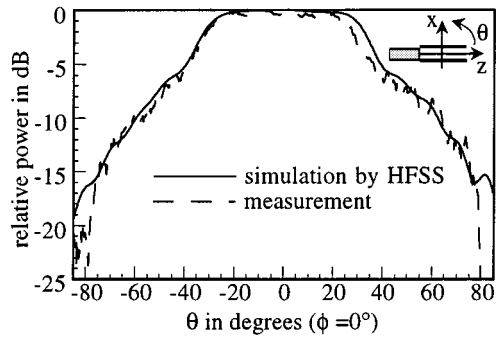

Fig. 9. Simulation and measurement of E-plane radiation patterns without the corrugated flares.

VI. Experimental Setup and Measurements

As illustrated in Fig. 7, the entire antenna is composed of the 50-mm APWLL, a pair of rotationally symmetric corrugated flares, and the H-plan sectional horn for a primary feed. Since the antenna is rotationally symmetric, the performance of the antenna is independent of the position of the feed. That is, the antenna has a wide scan angle. Also electronic beam switching would be possible.

Fig. 8 illustrates radiation patterns measured with three different scan angles 0°, 10°, and 20° in the H-plane without the flares (with only the APWLL). By simply turning the APWLL only, measurements of beam scan are taken. They verify that the APWLL antenna has a wide scan angle in azimuth and the PBG structure has nearly an isotropic property, as expected. The HPBW of the antenna is 5.2°, the first sidelobe is -17 dB. Fig. 8 also shows the simulation result. Compared with the simulation result, the measurements have a minimal increase of the HPBW and sidelobes. The reason is that edge diffractions by the front posts where the waves leave the APWLL disturb wave propagation and cause phase differences on the aperture. The measured cross polarization is very low.

In Fig. 9, two E-plane radiation patterns are illustrated. The simulation of the APWLL with 5.1λ diameter by HFSS is very well consistent with the measurement.

The antenna is also measured with the symmetric corrugated flares. The measurements in Fig. 10 show that the antenna has also a wide scan angle in azimuth like the APWLL antenna without the flares. The HPBW is 4.8° and the first sidelobe is -20 dB. However, if compared with the antenna without

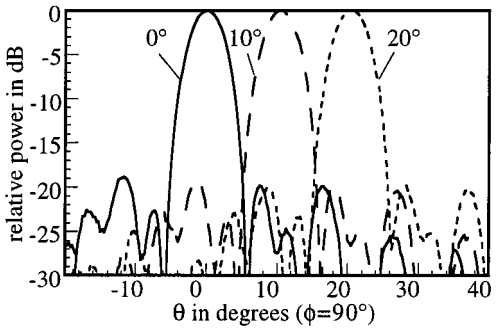

Fig. 10. H-plane radiation patterns for three different scan angles with the corrugated flares (see Fig. 7).

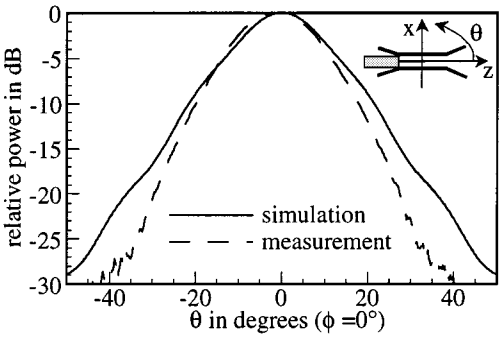

Fig. 11. Simulation and measurement with the corrugated flares in E-plane.

the flares, the antenna with the flares has about 0.4° narrower HPBW and −2.5-dB lower first sidelobe. The reason is that the symmetric corrugated flares remove the edge diffractions in both elevation and azimuth.

In Fig. 11, both simulation and measurement of E-plane radiation pattern are illustrated. Sidelobe levels are lower than −27 dB due to the corrugated flares. The HPBW is 19.5°. In terms of the HPBW, both the measurement and the simulation are in good agreement. Since the aperture becomes larger and the HPBW becomes narrower by adding the flares, the directivity of the entire antenna is about 6 dB higher than that of the APWLL without the flares.

By measuring S_{21} of the entire antenna, the coupling between two feeds is investigated. As a port 2, a open WR-10 waveguide is used. The S_{21} measurements are taken at different angles 150°, 120°, and 90° with the feed horn as a port 1 fixed at $\theta = 180°$. S_{21} is lower than −30 dB. Also, a S_{11} of −13 dB for the APWLL antenna is measured, but because of the corrugated flares, S_{11} for the complete antenna is −14 dB.

The gain of the antenna is measured by comparing the maximum value with that of the reference horn. The gains of the entire antenna and the APWLL are 23.5 and 17.5 dBi, respectively.

VII. Conclusion

A PBG structure for guiding surface waves in a parallel-plate waveguide is proposed. The design and fabrication procedure of the antenna with the 50-mm APWLL for a 76.5-GHz ACC radar are described in details. Measurements verify that the PBG structure in the APWLL works well like an artificial dielectric and also show that the simulation results are in good agreement with measurements. Due to the metallic fabrication of the APWLL, the entire antenna is mechanically stable and has no dielectric losses. Since the APWLL is implemented with the PBG in a parallel-plate waveguide, the antenna has very low profile in azimuth. It is expected that the antenna in this paper will be also applied to point-to-multipoint communications due to multiple beam's property. Lenses of different diameters, from 25 to 85 mm have been developed. All show comparable features.

References

[1] E. Yablonovitch, "Photonic band-gap structures," *J. Opt. Soc. Amer. B, Opt. Phys.*, vol. 10, no. 2, pp. 283–294, Feb. 1993.
[2] D. Sievenpiper, L. Zhang, R. F. Jimenez Broas, N. G. Alexópoulos, and E. Yablonovitch, "High-impedance electromagnetic surfaces with a forbidden frequency band," *IEEE Trans. Microwave Theory Tech.*, vol. 47, pp. 2059–2074, Nov. 1999.
[3] F.-R. Yang, K.-P. Ma, Y. Quin, and T. Itoh, "A novel TEM waveguide using uniplanar compact photonic-bandgap (UC-PBG) structure," *IEEE Trans. Microwave Theory Tech.*, vol. 47, pp. 2092–2098, Nov. 1999.
[4] J. D. Shumpert, W. J. Chappell, and L. P. B. Katehi, "Parallel-plate mode reduction in conductor-backed slots using electromagnetic bandgap substrates," *IEEE Trans. Microwave Theory Tech.*, vol. 47, pp. 2099–2104, Nov. 1999.
[5] R. E. Collin, *Field Theory of Guided Waves*, 2nd ed. New York: IEEE, 1991.
[6] R. S. Elliott, *Antenna Theory and Design*. Englewood Cliffs, NJ: Prentice-Hall, 1981, pp. 440–453.
[7] R. C. Johnshon and H. Jasik, *Antenna Engineering Handbook*, 2nd ed. New York: McGraw-Hill, 1984, ch. 12.
[8] P.-S. Kildal, "Artificially soft and hard surfaces in electromagnetics," *IEEE Trans. Antennas Propagat.*, vol. 38, pp. 1537–1544, Oct. 1990.
[9] L. Brillouin, "Wave guides for slow waves," *J. Appl. Phys.*, vol. 19, pp. 1023–1041, 1948.
[10] R. Schneider, "Modellierung der Wellenausbreitung für ein bildgebendes Kfz-Radar," Ph.D. dissertation, Univ. Karlsruhe, Karlsruhe, Germany, 1998.
[11] R. K. Luneburg, *Mathematical Theory of Optics*. Berkeley, CA: Univ. California Press, 1964.
[12] R. C. Hansen, *Microwave Scanning Antennas*. New York: Academic, 1964, vol. 1, pp. 224–233.
[13] R. J. King, D. V. Thiel, and K. S. Park, "The synthesis of surface reactance using an artificial dielectric," *IEEE Trans Antennas Propagat.*, vol. AP-31, pp. 471–476, May 1983.
[14] C. H. Walter, "Surface-wave Luneburg lens antennas," *IEEE Trans. Antennas Progagat.*, vol. AP-8, pp. 508–515, Sept. 1960.
[15] R. F. Harrington, *Time-Harmonic Electromagnetic Fields*. New York: McGraw-Hill, 1961, pp. 158–171.
[16] M. Vogel, "Theoretische und experimentelle Untersuchungen zur quasioptischen Abbildung mit Millimeterwellen, insbesondere mit Luneburg Linsen," Fortschritt-Ber. VDI-Z., Reihe 10, Tech. Rep. 14, 1982.
[17] C. A. Mentzer and JR. Leon Peters, "Pattern analysis of corrugated horn antennas," *IEEE Trans. Antennas Propagat.*, vol. AP-24, pp. 304–309, May 1976.
[18] ——, "Properties of cutoff corrugated surfaces for corrugated horn design," *IEEE Trans. Antennas Propagat.*, vol. AP-22, pp. 191–196, Mar. 1974.

Young-Jin Park (S'99) was born in Masan, Korea, on January 7, 1971. He received the B.S. degree from Chung-Ang University, Seoul, Korea, in 1997, the M.S. degree in electrical engineering from the Korea Advanced Institute of Science and Technology (KAIST), Taejon, Korea, in 1999, and is currently working toward the Dr.-Ing. degree at the Institut für Höchstfrequenztechnik und Elektronik (IHE), University of Karlsruhe, Karlsruhe, Germany.

His research interests include millimeter-wave antennas, PBG structures, and adaptive cruise control (ACC) radar.

Alexander Herschlein was born in Heilbronn, Germany, on October 21, 1966. He received the Dipl.Ing. degree in electrical engineering from the University of Karlsruhe, Karlsruhe, Germany, in 1993, and is currently working toward the Dr.-Ing. degree at the Institut für Höchstfrequenztechnik und Elektronik (IHE), University of Karlsruhe.

His research interests include adaptive cruise control (ACC) radar, millimeter-wave antennas, and numerical analysis of electromagnetic compatibility and conformal antennas.

Werner Wiesbeck (SM'87–F'94) received the Dipl.-Ing. (M.S.E.E.) and the Dr.-Ing. (Ph.D.E.E.) degrees from the Technical University Munich, Germany, in 1969 and 1972, respectively.

From 1972 to 1983, he was with AEG-Telefunken in various positions including Head of R&D of the Microwave Division in Flensburg and Marketing Director Receiver and Direction Finder Division, Ulm. During this period, he had product responsibility for millimeter-wave radars, receivers, direction finders, and electronic warfare systems. Since 1983, he has been Director of the Institut für Höchstfrequenztechnik und Elektronik (IHE), University of Karlsruhe. Research topics include radar, remote sensing, wave propagation, and antennas. In 1989 and 1994, respectively, he spent a six-month sabbatical at the Jet Propulsion Laboratory, Pasadena, CA.

Dr. Wiesbeck is a member of the IEEE GRS-S AdCom (1992–2000), Chairman of the GRS-S Awards Committee (1994–1998), Executive Vice President IEEE GRS-S (1998–1999), President IEEE GRS-S (2000–2001), Associate Editor IEEE TRANSACTIONS ON ANTENNAS AND PROPAGATION (1996–1999), and past Treasurer of the IEEE German Section (1987–1996). He has been General Chairman of the 1988 Heinrich Hertz Centennial Symposium, the 1993 Conference on Microwaves and Optics (MIOP 1993). He has also been a member of the scientific committees of many conferences. For the Carl Cranz Series for Scientific Education, he serves as a permanent lecturer for radar system engineering and for wave propagation. He is a member of an Advisory Committee of the EU-Joint Research Centre (Ispra/Italy). He is an advisor to the German Research Council (DFG), to the Federal German Ministry for Research (BMBF), and to industry in Germany.